A VISCOUS TWO-PHASE MODEL FOR CONTRACTILE ACTOMYOSIN BUNDLES.

DIETMAR OELZ

Abstract. A mathematical model in one dimension for a non-sarcomeric actomyosin bundle featuring anti-parallel flows of anti-parallel F-Actin is introduced. The model is able to relate these flows to the effect of cross-linking and bundling proteins, to the forces due to myosin-II filaments and to external forces at the extreme tips of the bundle.

The modeling is based on a coarse graining approach starting with a microscopic model which includes the description of chemical bonds as elastic springs and the force contribution of myosin filaments. In a second step we consider the asymptotic regime where the filament lengths are small compared to the overall bundle length and restrict to the lowest order contributions. There it becomes apparent that myosin filaments generate forces which are partly compensated by drag forces due to cross-linking proteins. The remaining local contractile forces are then propagated to the tips of the bundle by the viscosity effect of bundling proteins in the filament gel.

The model is able to explain how a disordered bundle of comparatively short actin filaments interspersed with myosin filaments can effectively contract the two tips of the actomyosin bundle. It gives a quantitative description of these forces and of the anti-parallel flows of the two phases of anti-parallel F-Actin. An asymptotic version of the model with infinite viscosity can be solved explicitly and yields an upper bound to the contractile force of the bundle. Actomyosin and F-Actin bundle and Contractility and Free boundary problem and Active fluid 92C10 and 35Q92

1. Introduction

Mechanical force generated by biological cells is often generated by the interplay of myosin-II molecular motors and actin filaments. In striated muscle cells the actomyosin system is highly structured and well understood starting with the pioneering modeling works of A.F. Huxley ([16]). Force generation in actomyosin bundles featuring a sarcomeric structure works similarly (see eg. [6]). How actin and myosin-II filaments cooperate in actomyosin bundles with less structure like smooth muscle fibers ([11]), stress fibers with graded polarity ([10]), the contractile ring in cytokinesis ([7]) and the rear bundle in keratocytes ([33]), however, is a field of ongoing research.

Actin is a polar protein which forms lengthy filaments termed F-Actin. Actin filaments are also polar with their so called barbed end as opposed to the so called pointed end. Myosin-II is an ATP-dependent motor protein which contains two heavy chains. The head domains containing the motor are kept in close proximity by wrapping of the two tail domains. Cytoplasmic myosin-II dimers aggregate further through their tail regions to form bipolar thick filaments with the head regions

Date: Received: date / Accepted: date.

pointing outside of the filament ([1]). In a geometrical configuration as visualized in figure 1, where a myosin-II protein is parallelly aligned to an actin fiber with its head domains pointing in the direction of the barbed end of the actin fiber, ATP-dependent power strokes are performed. Myosin-II in such a configuration acts as a molecular motor and a force is generated by which a myosin filament moves along the actin filament towards its barbed end (cf. [37, 13]).

We refer to an ensemble of interacting actin and myosin-II filaments as an actomyosin system. They include non-directed, mesh-like ones as the cell cortex and myosin filaments interspersed in the lamellipodial actin filament mesh-work as well as directed ones, i.e. actin filaments and myosin filaments arranged in bundles. In bundles the forces generated by myosin heads might cause internal flows and also changes in total length of the bundle. For example in [18] it was found that stress fibers shorten due to the contractility of the actomyosin system rather than by depolymerization of actin filaments. Stress fibers which feature a sarcomeric structure have been identified ([22]) as well as stress fibers lacking such a structure ([10]).

Apart from the interaction with myosin-II bipolar filaments, actin filaments might be connected by cross-linking and bundling proteins. Cross-linking proteins are filamin ([39]) and α-actinin which targets filaments crossing over all angles ([9]). A bundling protein is fascin ([17]) which predominantly links parallel filaments ([9]). In bundles mostly α-actinin and fascin can be found, whereas filamin is almost exclusively present in mesh-works ([9]).

Since in this study we concentrate on non-sarcomeric actomyosin bundles we also mention that minimal non-sarcomeric contractile actomyosin bundles have been recently reconstituted in vitro in [34]. Nevertheless, the internal structure of non-sarcomeric actomyosin bundles and minimal requirements of contractility are open questions.

1.1. **State of the Art.** Models on non-directed actomyosin networks include phenomenological models for the contractile effect of myosin-II filaments in a continuous medium ([31, 3]) as well as the two component, isotropic continuum description of a cytoskeletal network coupled to contractile stress caused by molecular motors which has been formulated in [24].

As far as models on actomyosin bundles are concerned many models focus on the details of force generation (e.g. [4]). The idea of F-Actin flowing with the bundle has been formulated in a qualitative model published in [30].

Other studies focus on the structure of actomyosin system in bundles. A schematic picture of stress fibers as an ordered (sarcomeric) bundle of parallel polar actin filaments interspersed with bipolar myosin-II filaments and α-actinin and filamin as cross-linkers has been shown in [22]. Detailed modeling with a focus on the twisted geometry of actin filaments has been undertaken in [15]. Changes in the mechanical regime of actomyosin bundles due to cross-linking and bundling by α-actinin and fascin have been investigated in [36] and simulated in [35].

A model which describes the mechanical aspects of sarcomeric actomyosin bundles by a linear chain of dash-pot models has been introduced in [5] and a continuum limit (cf. [6]) has been performed which was applied in [8] revealing the contractile profile in stress fibers and bidirectional sliding of actin filaments.

Concerning non-sarcomeric bundles, a general framework for the description of parallel polar filaments which interact through motor proteins has been introduced

in [21] in a one dimensional setting. The same authors had already presented a minimal model in [20] which investigates the emergence of contractility and tension in non-sarcomeric bundles. The model, however, is phenomenological and primarily macroscopic as it does not describe details of the polymerization and depolymerization processes which would involve describing the length-distribution of filaments.

Finally a microscopic model for non-sarcomeric bundles which carefully describes a microscopic picture of an actomyosin ensemble has been presented in [23]. It does, however, not allow for a dynamic remodeling of cross-linker connections and therefore resorts to buckling of single actin filaments as a consequence of contractile forces.

1.2. **Purpose and outline of this study.** The present study presents a coarse-graining modeling approach which allows to identify the mandatory constituents of a contractile disordered actomyosin system. Its primary concern is to explain how the locally generated myosin dependent contractile forces are integrated to effectuate the contractile force acting at the tips of the bundle. It closes with the formulation of an asymptotic limit of that model which allows to compute the contractile force explicitly. It is shown that the effect of bundling proteins is essential for the propagation of the locally generated contractile force to the bundle tips.

The outline of this study is as follows. First we introduce a microscopic description of an actomyosin assemble including cross-linker and bundling proteins. In this formulation we do not talk about the tips of the bundle. Next we pass to an asymptotic limit of small filament lengths. In this formulation the tips of the bundle can be localized which is done in the next step.

Finally two alternative approaches to use the model are presented: One where the contractile force is fixed and where the solution of the model allows to evaluate the change in bundle length. The other approach fixes the bundle length and allows to obtain the contractile force from the solution of the model. Finally we evaluate the explicit formula for the contractile force which we obtain in the special asymptotic limit case where the effect of bundling proteins dominates.

2. Microscopic model for actomyosin bundle

We consider a bundle of polar actin filaments interspersed with bipolar myosin-II filaments (cf. [33]). We describe the position of filaments along the bundle by two scalar values which denote the position of the barbed end and of the pointed end along the real line. We do not take into account the position of a given filament within the cross section of a bundle.

We distinguish between filaments which have their pointed ends to the right (and their barbed ends to the left) denoting them with superscript $^+$ and index $i \in I$. This refers to the fact that due to the action of myosin-II filaments they will typically move to the right relative to the bundle.

For the filaments which have their pointed ends to the left (and thus their barbed ends to the right) on the other hand we use symbols with superscripts $^-$ and index $j \in J$.

Hence $b_i^+(t) < p_i^+(t)$ denote the positions of the barbed end and the pointed end of the right-moving filament with index i as functions of time $t \geq 0$. Analogously the barbed end and pointed end of the left-moving filament with index j are denoted by $b_j^-(t) > p_j^-(t)$.

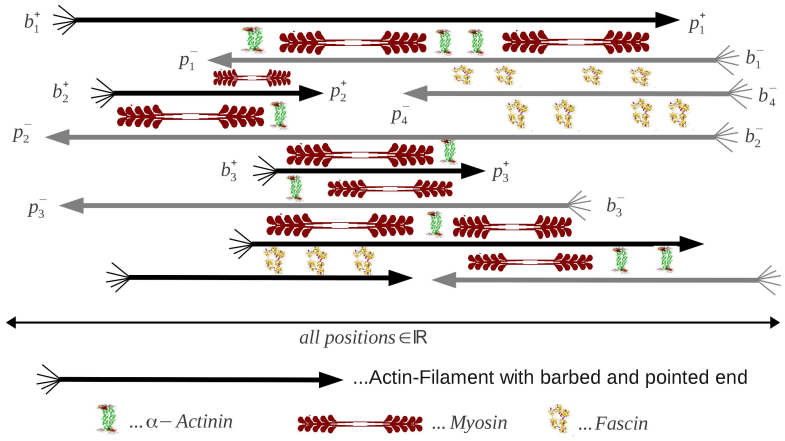

FIGURE 1. Constituents of the microscopic model.

Additionally we describe polymerization of filaments at the barbed end by given filament specific rates $v_{p,i}^+(t)$ and $v_{p,j}^-(t)$ respectively. Depolymerization at the pointed ends with rates $v_{d,i}^+(t)$ and $v_{d,j}^-(t)$ is also taken into account. We define the material velocities of right and left-moving filaments.

$$\begin{aligned} \bar{v}_i^+ &:= \partial_t p_i^+ + v_{d,i}^+ = \partial_t b_i^+ + v_{p,i}^+ \,, \\ \bar{v}_j^- &:= \partial_t p_j^- - v_{d,j}^- = \partial_t b_j^- - v_{p,j}^- \,, \end{aligned} \tag{1}$$

where the two identities hold since only polymerization and depolymerization may change the length of a given actin filament.

Key issue to the model we develop is the force which is transmitted between overlapping actin filaments. Internal forces may act due to myosin-II filaments, cross-linking proteins or bundling proteins and the magnitude of these forces will typically be proportional to the length of the interval within which two interacting actin filaments overlap.

To quantify the length of such an overlapping region we consider two actin filaments with endpoints at $a < b$ and at $c < d$ respectively, without specifying whether they belong to the right or left-moving group. The length of the interval in which they overlap can then be computed by

$$L_{(c,d)}^{(a,b)} := |(a,b) \cap (c,d)| = (\min(b,d) - \max(c,a))_+ \,.$$

Since we do not take into account the position of a given filament within the cross section of a bundle we have to be careful talking about the interaction of single filaments when the bundle contains more than a few actin filaments. In such a case the probability by which two actin filaments, which overlap in the interval $(\max(c,a), \min(b,d))$, actually are nearby and therefore typically will interact, is inversely proportional to the total number of filaments which can be found in that interval. We quantify the latter approximately by

$$N^{(\alpha,\beta)} := \frac{\sum_i L_{(b_i^+, p_i^+)}^{(\alpha,\beta)} + \sum_j L_{(p_j^-, b_j^-)}^{(\alpha,\beta)}}{\beta - \alpha} \,, \tag{2}$$

which actually compares the length of all the F-actin material located in the given interval (α, β) to its length. We define the additional coefficient, which we call probability of neighborhood, by

$$P^{(a,b)}_{(c,d)} = \frac{\nu}{N^{(\max(c,a),\min(b,d))}} ,$$

where the coefficent $\nu > 0$ is a geometric parameter and represents the typical number of neighboring filaments that one specific filament would have within the cross section of a bundle. We implicitly use here the assumption that the number of filaments in the cross-section is larger than ν which guarantees that $P^{(a,b)}_{(c,d)} < 1$.

The product of the two scalar values for the length of the overlapping region and the probability of neighborhood finally gives an effective interaction length for two filaments located at (a, b) and (c, d) respectively,

$$A^{(a,b)}_{(c,d)} = L^{(a,b)}_{(c,d)} P^{(a,b)}_{(c,d)} , \tag{3}$$

which we will use in the computation of any force acting between two filaments.

We assume that the bundle is in an over-damped regime and formulate a preliminary microscopic model as a system of force balance equations given by

$$0 = \sum_j A^{(p_j^-, b_j^-)}_{(b_i^+, p_i^+)} \left(\eta^{\mathrm{myo}} - \eta^{\mathrm{cl}} \left(\bar{v}_i^+ - \bar{v}_j^- \right) \right) - \sum_{\bar{i}} A^{(b_i^+, p_i^+)}_{(b_{\bar{i}}^+, p_{\bar{i}}^+)} \eta^{\mathrm{bdl}} \left(\bar{v}_i^+ - \bar{v}_{\bar{i}}^+ \right) + f_i^+ \tag{4}$$

and

$$0 = - \sum_i A^{(p_j^-, b_j^-)}_{(b_i^+, p_i^+)} \left(\eta^{\mathrm{myo}} - \eta^{\mathrm{cl}} \left(\bar{v}_i^+ - \bar{v}_j^- \right) \right) - \sum_{\bar{j}} A^{(p_j^-, b_j^-)}_{(p_{\bar{j}}^-, b_{\bar{j}}^-)} \eta^{\mathrm{bdl}} \left(\bar{v}_j^- - \bar{v}_{\bar{j}}^- \right) + f_j^- . \tag{5}$$

In (4) the index i of a right-moving filament is fixed and forces acting on that filament are being described. In the same way (5) refers to a left-moving filament with a fixed index j. The force balance is established between the time dependent exterior force $f_i^+(t)$ and $f_j^-(t)$ respectively and forces between the respective filament and other filaments of both orientations.

The idea behind the formulation of exterior forces is that cytoskeleton structures which are not part of the model will attach to actin filaments within the bundle. In a later step of the model derivation we will assume that such connections only exist at the two far ends of the bundle. What we have in mind are linkages to the surrounding actin cytoskeleton by which contractile forces are being transmitted.

The force which is generated by myosin-II filaments between two filaments of opposite direction is modeled by an effective force coefficient η^{myo} multiplied by the effective interaction length (3). We refer to appendix B for more details about the derivation of this macroscopic parameter with dimension $[\eta^{\mathrm{myo}}] = \text{force/length}$.

The force between actin filaments of opposite direction mediated by cross-linking proteins is modeled as a drag force and therefore proportional to an effective coefficient η^{cl}, to the relative velocity of the two filaments and to the effective interaction length. The relative velocity is given as the difference of the two material velocities (1). When we talk about cross-linking proteins we have mostly α-actinin in mind. We refer to appendix B for a derivation of η^{cl} ($[\eta^{\mathrm{cl}}] = \text{force/(velocity} \times \text{length)}$) from microscopic data on α-actinin structure and binding dynamics along the lines of the approach presented in [26].

Finally the force between filaments of the same direction mediated by bundling proteins is also modeled as a drag force, this time comparing the speed of movement of one filament to that of all those filaments with the same direction of movement. The effective coefficient related to the drag force is written as $\eta^{\rm bdl}$ with physical dimension $[\eta^{\rm bdl}] = \text{force}/(\text{velocity} \times \text{length})$. Its derivation from microscopic data on fascin is analogous to the derivation of $\eta^{\rm cl}$.

Observe that for finite numbers of right and left-moving filaments and given the exterior forces $f_i^+(t)$ and $f_j^-(t)$ and the polymerization and depolymerization rates $v_{p,i}^+(t)$, $v_{d,i}^+(t)$, $v_{p,j}^-(t)$ and $v_{d,j}^-(t)$ the system of equations (1), (4) and (5) forms a closed ODE-system for the positions of the barbed and pointed ends $b_i^+(t)$, $p_i^+(t)$, $b_j^-(t)$ and $p_j^-(t)$.

3. Derivation of the asymptotic limit model

3.1. **Continuous description.** We further process the model in two steps. First we pass to a continuous description based on density functions. Next, we consider an asymptotic regime, where the typical length of actin filaments is small compared to the total length of the bundle.

We start by applying a coordinate transformation by which we replace the two endpoints of a filament by its center point and its length. The new variables for the right-moving and the left-moving filaments are given by

$$(x_i^+, l_i^+) = \left(\frac{p_i^+ + b_i^+}{2}, p_i^+ - b_i^+ \right) \quad \text{and} \quad (x_j^-, l_j^-) = \left(\frac{p_j^- + b_j^-}{2}, b_j^- - p_j^- \right) , \tag{6}$$

which guarantees $l_i^+ \geq 0$ and $l_j^- \geq 0$. We also introduce a modified notation for the effective interaction coefficient

$$\bar{A}^{(x,l)}_{(\bar{x},\bar{l})} := A^{(x-l/2, x+l/2)}_{(\bar{x}-\bar{l}/2, \bar{x}+\bar{l}/2)}$$

and write the microscopic model (4), (5) as

$$0 = \sum_j \bar{A}^{(x_j^-, l_j^-)}_{(x_i^+, l_i^+)} \left(\eta^{\rm myo} - \eta^{\rm cl} \left(\bar{v}_i^+ - \bar{v}_j^- \right) \right) - \sum_{\bar{i}} \bar{A}^{(x_i^+, l_i^+)}_{(x_{\bar{i}}^+, l_{\bar{i}}^+)} \, \eta^{\rm bdl} \left(\bar{v}_i^+ - \bar{v}_{\bar{i}}^+ \right) + f_i^+ \tag{7}$$

and

$$0 = - \sum_i \bar{A}^{(x_j^-, l_j^-)}_{(x_i^+, l_i^+)} \left(\eta^{\rm myo} - \eta^{\rm cl} \left(\bar{v}_i^+ - \bar{v}_j^- \right) \right) - \sum_{\bar{j}} \bar{A}^{(x_j^-, l_j^-)}_{(x_{\bar{j}}^-, l_{\bar{j}}^-)} \, \eta^{\rm bdl} \left(\bar{v}_j^- - \bar{v}_{\bar{j}}^- \right) + f_j^- , \tag{8}$$

with the material velocities (1) written as

$$\begin{aligned} \bar{v}_i^+ &:= \partial_t x_i^+ + \frac{v_{d,i}^+ + v_{p,i}^+}{2} , \\ \bar{v}_j^- &:= \partial_t x_j^- - \frac{v_{d,j}^- + v_{p,j}^-}{2} . \end{aligned} \tag{9}$$

A continuous description of an infinite number of filaments is obtained by formulating the Eulerian description of the bundle introducing the densities $\rho^+(t,x,l)$ and $\rho^-(t,x,l)$ of filaments moving to the right and to the left respectively. Note that ρ^+ and ρ^- are considered time dependent number densities per filament length and per bundle length unit. In the following we write usually two equations in once.

The one with the upper symbols refers to those filaments moving to the right and the one with the lower symbols to those moving to the left. We introduce the fluxes

$$U^{\pm}(t,x,l) = \begin{pmatrix} V^{\pm}(t,x,l) \\ G^{\pm}(t,x,l) \end{pmatrix} ,$$

where $V^{+}(t,x,l)$ and $G^{+}(t,x,l)$ represent $\partial_t x_i^{+}$ and $\partial_t l_i^{+}$ respectively of right-moving filaments located in an infinitesimally small interval around x with lengths in an infinitesimally small interval around l. The analogous interpretation applies to $V^{-}(t,x,l)$ and $G^{-}(t,x,l)$. Especially for the flux in the dimension of filament lengths it holds that

$$G^{\pm}(t,x,l) \quad = \quad v_p^{\pm} - v_d^{\pm} .$$

Here the polymerization and depolymerization rates $v_p^{\pm}$ and $v_d^{\pm}$ are considered as functions of (t,x) replacing their respective discrete versions. The material velocities (9) taking into consideration polymerization and depolymerization are now written as

$$\bar{V}^{\pm} := V^{\pm} \pm \frac{1}{2}\left(v_p^{\pm} + v_d^{\pm}\right) .$$

Reformulated in terms of the new quantities the model combines continuum equations for the two families of filaments

$$\partial_t \rho^{\pm} + \frac{\partial}{\partial x}\left(V^{\pm}\rho^{\pm}\right) + \frac{\partial}{\partial l}\left(G^{\pm}\rho^{\pm}\right) = 0 \tag{10}$$

with the reformulated versions of the force balance laws (4) and (5) determining the fluxes

$$\begin{aligned} 0 = \int_{\mathbb{R}}\int_0^{\infty} \bar{A}^{(x,l)}_{(\bar{x},\bar{l})}\left(\pm\eta^{\mathrm{myo}} - \eta^{\mathrm{cl}}\left(\bar{V}^{\pm}(t,x,l) - \bar{V}^{\mp}(t,\bar{x},\bar{l})\right)\right)\rho^{\mp}(t,\bar{x},\bar{l})\, d\bar{l}\, d\bar{x} - \\ - \int_{\mathbb{R}}\int_0^{\infty} \bar{A}^{(x,l)}_{(\bar{x},\bar{l})}\,\eta^{\mathrm{bdl}}\left(\bar{V}^{\pm}(t,x,l) - \bar{V}^{\pm}(t,\bar{x},\bar{l})\right)\rho^{\pm}(t,\bar{x},\bar{l})\, d\bar{l}\, d\bar{x} + \\ + f^{\pm}(t,x,l) . \end{aligned} \tag{11}$$

Observe that (11) is a system which holds pointwise at $(x,l) \in \mathbb{R}\times\mathbb{R}^{+}$. It describes a force balance where the specific forces like for example the external forces $f^{\pm}(t,x,l)$ are interpreted as though they acted on one filament centered within an infinitesimal volume element around $(x,l) \in \mathbb{R}\times\mathbb{R}^{+}$. Note also that the system consisting of (11) and of a weak formulation of (10) is equivalent to the discrete models formulated at first when the density functions are taken as point measures $\rho^{+} = \sum_i \delta(x-x_i(t))\delta(l-l_i(t))$ and the equivalent expressions for the left-moving filaments corresponding to empirical distributions.

3.2. **Asymptotic limit.** In the following we intend to pass to an asymptotic limit, where the typical length of actin filaments becomes small. To this end we introduce the following rescaled dimensionless versions of the independent and dependent variables as well as of the parameters for the drag forces and the myosin force.

$$l = l_0\,\tilde{l}\,, \quad x = x_0\,\tilde{x}\,, \quad t = t_0\,\tilde{t}\,, \quad \varepsilon = \frac{l_0}{x_0}\,,$$

$$\rho^{\pm}(t_0\tilde{t}, x_0\tilde{x}, l_0\,\tilde{l}) = \frac{1}{\varepsilon}\frac{1}{l_0\;x_0}\tilde{\rho}^{\pm}(\tilde{t},\tilde{x},\tilde{l})\,, \quad V^{\pm} = \frac{x_0}{t_0}\tilde{V}^{\pm}\,, \quad G^{\pm} = \frac{l_0}{t_0}\tilde{G}^{\pm}\,,$$

$$\eta^{\rm myo} = \frac{f_0}{x_0}\tilde\eta^{\rm myo}\ , \quad \eta^{\rm cl} = \frac{f_0 t_0}{x_0^2}\tilde\eta^{\rm cl}\ , \quad \eta^{\rm bdl} = \frac{1}{\varepsilon^2}\frac{f_0 t_0}{x_0^2}\tilde\eta^{\rm bdl}\ ,$$

$$f^\pm(t_0\tilde t, x_0\tilde x, l_0\tilde l) = \varepsilon f_0\, \tilde f^\pm(\tilde t,\tilde x,\tilde l)\ , \quad v^\pm_{p/d}(t_0\tilde t, x_0\tilde x) = \frac{l_0}{t_0}\tilde v^\pm_{p/d}(\tilde t,\tilde x)\ ,$$

where f_0, t_0, x_0, l_0 are reference values for the forces, the timescale of the model, the length of the bundle and the length of the filaments. Observe that as a consequence the scaled material fluxes $\bar V^\pm = \frac{x_0}{t_0}\tilde{\bar V}^\pm$ satisfy

$$\tilde{\bar V}^\pm = \tilde V^\pm \pm \frac{\varepsilon}{2}\left(\tilde v_p^\pm + \tilde v_d^\pm\right)\ .$$

The dimensionless parameter ε represents the ratio of the typical filament length vs. typical bundle length. To maintain the total amount of F-Actin when ε becomes small, we assume that the filament densities are of the order $1/\varepsilon$ meaning that as the filament lengths get small the abundance of actin filaments increases. Hence the concentration density of F-Actin given by the first moments $\int_0^\infty l\rho^\pm\, dl$ are of order 1. External forces on the other hand scale like ε to maintain the total amount of external forces on a steady level when the total number of filaments gets large. The scalings of the macroscopic parameters $\eta^{\rm myo}$, $\eta^{\rm cl}$ and $\eta^{\rm bdl}$ with respect to ε are chosen in order to capture the leading order terms in the asymptotic expansion of the scaled version of (11) as ε becomes small: In (17) below it becomes apparent that the leading order term of the expressions which refer to bundling proteins are of second order whereas the leading order terms of those expressions refering to myosin-II filaments and cross-linker proteins are of order zero.

For notational convenience we omit the tildes again, but equip some of the dependent quantities with the subscript ε referring to the fact that this dimensionless parameter appears in the defining equations.

In the limit model moments of the limit filament distribution will play a central role, for which we introduce the short notation

$$\mu_k^\pm(t,x) := \int_0^\infty l^k\, \rho_0^\pm(t,x,l)\, dl \quad \text{for} \quad k = 0,1,2,3\ . \tag{12}$$

Below we will further comment the interpretation of these quantities. In Appendix A we collect some computations which imply the following asymptotic results for moments of the effective interaction length, which will be the main tool to derive the formal limit equation.

$$\int_{\mathbb{R}} \bar A^{(x,\varepsilon l)}_{(x+\Delta\bar x,\varepsilon\bar l)}\, d\Delta\bar x = \varepsilon^2\, \bar l\, l \frac{\nu}{\mu_1^+(t,x)+\mu_1^-(t,x)} + O(\varepsilon^3) \tag{13}$$

$$\int_{\mathbb{R}} \Delta\bar x\, \bar A^{(x,\varepsilon l)}_{(x+\Delta\bar x,\varepsilon\bar l)}\, d\Delta\bar x = \frac{\varepsilon^4}{12}\, \bar l\, l^3 \partial_x\left(\frac{\nu}{\mu_1^+(t,x)+\mu_1^-(t,x)}\right) + O(\varepsilon^5)\ , \tag{14}$$

$$\int_{\mathbb{R}} (\Delta\bar x)^2 \bar A^{(x,\varepsilon l)}_{(x+\Delta\bar x,\varepsilon\bar l)}\, d\Delta\bar x = \frac{\varepsilon^4}{12}\, \bar l\, l\, (l^2+\bar l^2) \frac{\nu}{\mu_1^+(t,x)+\mu_1^-(t,x)} + O(\varepsilon^5)\ . \tag{15}$$

Observe that for symmetry reasons (see Appendix A for details) the lowest order term of the first moment is not of third but of fourth order.

The system (11) reads after scaling

$$
\begin{aligned}
(16)\quad 0 = \frac{1}{\varepsilon}\iint \bar{A}^{(x,\varepsilon l)}_{(x+\Delta\bar{x},\varepsilon\bar{l})}\left(\pm\eta^{\mathrm{myo}} - \eta^{\mathrm{cl}}\left(\bar{V}^{\pm}_{\varepsilon}(t,x,l) - \bar{V}^{\mp}_{\varepsilon}(t,x+\Delta\bar{x},\bar{l})\right)\right)\times \\
\times\, \rho^{\mp}_{\varepsilon}(t,x+\Delta\bar{x},\bar{l})\, d\Delta\bar{x}\, d\bar{l} - \\
-\frac{1}{\varepsilon^3}\iint \eta^{\mathrm{bdl}}\bar{A}^{(x,\varepsilon l)}_{(x+\Delta\bar{x},\varepsilon\bar{l})}\left(\bar{V}^{\pm}_{\varepsilon}(t,x,l) - \bar{V}^{\pm}_{\varepsilon}(t,x+\Delta\bar{x},\bar{l})\right)\times \\
\times\, \rho^{\pm}_{\varepsilon}(t,x+\Delta\bar{x},\bar{l})\, d\Delta\bar{x}\, d\bar{l} + \varepsilon\, f^{\pm}\,,
\end{aligned}
$$

where we applied the transformation $\bar{x} = x + \Delta\bar{x}$. The leading order term is the one related to bundling proteins. We integrate (16) against $V^{\pm}(t,x,l)\,\rho^{\pm}(t,x,l)$, apply Taylor expansions and pass formally to the limit as $\varepsilon \to 0$ using the asymptotic result for the zeroth moment (13) obtaining

$$
\begin{aligned}
0 = \int \frac{\nu}{\mu_1^+(t,x)+\mu_1^-(t,x)}\iint l\,\bar{l}\,\left(V_0^{\pm}(t,x,l) - V_0^{\pm}(t,x,\bar{l})\right)\times \\
\times\, V_0^{\pm}(t,x,l)\,\rho_0^{\pm}(t,x,\bar{l})\,\rho_0^{\pm}(t,x,l)\, d\bar{l}\, dl\, dx\,.
\end{aligned}
$$

Symmetrization using the fact that we can switch the symbols $l \leftrightarrow \bar{l}$ implies that

$$
\begin{aligned}
0 = \int\Bigg[\frac{\nu}{\mu_1^+(t,x)+\mu_1^-(t,x)}\times \\
\times \iint l\,\bar{l}\,\left(V_0^{\pm}(t,x,l) - V_0^{\pm}(t,x,\bar{l})\right)^2\rho_0^{\pm}(t,x,\bar{l})\,\rho_0^{\pm}(t,x,l)\, d\bar{l}\, dl\Bigg] dx\,,
\end{aligned}
$$

which implies that $V_0^{\pm}(t,x,l) = V_0^{\pm}(t,x,\bar{l})$ a.e. on $\mathbb{R}\times\mathbb{R}^2_+$ (or less according to the support of $\rho_0^{\pm}$). Hence we state that in the limit the velocities do not depend on the filament length,

$$
V_0^{\pm}(t,x,l) = V_0^{\pm}(t,x)\,.
$$

on the support of $\rho_0^{\pm}$.

With a view to pass to a macroscopic description omitting the dependence on filament lengths, we integrate (16) against $\rho^{\pm}_{\varepsilon}(t,x,l)$ obtaining

$$
\begin{aligned}
(17)\quad 0 = \frac{1}{\varepsilon}\iiint \bar{A}^{(x,\varepsilon l)}_{(x+\Delta\bar{x},\varepsilon\bar{l})}\left(\pm\eta^{\mathrm{myo}} - \eta^{\mathrm{cl}}\left(\bar{V}^{\pm}_{\varepsilon}(t,x,l) - \bar{V}^{\mp}_{\varepsilon}(t,x+\Delta\bar{x},\bar{l})\right)\right)\times \\
\times\, \rho^{\mp}_{\varepsilon}(t,x+\Delta\bar{x},\bar{l})\,\rho^{\pm}_{\varepsilon}(t,x,l)\, d\Delta\bar{x}\, dl\, d\bar{l} - \\
-\frac{1}{\varepsilon^3}\iiint \eta^{\mathrm{bdl}}\bar{A}^{(x,\varepsilon l)}_{(x+\Delta\bar{x},\varepsilon\bar{l})}\left(\bar{V}^{\pm}_{\varepsilon}(t,x,l) - \bar{V}^{\pm}_{\varepsilon}(t,x+\Delta\bar{x},\bar{l})\right)\times \\
\times\, \rho^{\pm}_{\varepsilon}(t,x+\Delta\bar{x},\bar{l})\,\rho^{\pm}_{\varepsilon}(t,x,l)\, d\Delta\bar{x}\, dl\, d\bar{l} + \varepsilon\int_0^{\infty} f^{\pm}\rho^{\pm}_{\varepsilon}(t,x,l)\, dl\,.
\end{aligned}
$$

We apply a Taylor series expansion in the x-variable to all those terms which involve $\Delta\bar{x}$ and pass to the limit as $\varepsilon \to 0$. What before were the leading order terms now cancel and from the $O(\varepsilon)$ equations we obtain using the asymptotic

result for the moments (13)-(15)

$$0 = \left(\pm\eta^{\mathrm{myo}} - \eta^{\mathrm{cl}}\left(V_0^{\pm} - V_0^{\mp}\right)\right)\frac{\nu\mu_1^+\mu_1^-}{\mu_1^+ + \mu_1^-} + \\ + \eta^{\mathrm{bdl}}\frac{1}{12}\,\partial_x\left(\partial_x V_0^{\pm}\frac{\nu\mu_1^{\pm}\mu_3^{\pm}}{\mu_1^+ + \mu_1^-}\right) + \int_0^{\infty} f^{\pm}\,\rho_0^{\pm}\,dl \tag{18}$$

as the macroscopic limit of the original microscopic force balance laws (4) and (5) coupled to the continuity equations (10), which even after scaling remain unchanged.

Under the simplifying assumption $G_0^{\pm}(t,x,l) = G_0^{\pm}(t,x)$ one could derive from (10) a system of moments up to third order. However, that system of four equations would still not be closed since it includes $\rho_0^{\pm}(t,x,l=0)$. For this reason we prefer to work directly with the full continuity equation (10) in the rest of this study.

The most striking feature of the limit equation (18), besides its apparent simplicity compared to the original integral equation (16), is the fact the third moments of the limit distributions (12) appear in the viscosity coefficient.

It is much easier to understand the appearance of the first moments $\mu_1^{\pm}(t,x)$ which represent the F-Actin density measured in total length of Actin fibers per bundle unit length (or, after multiplication by a corresponding proportionality constant, mass per unit length or mol G-Actin per unit length). It is intuitive that in the limit model (18) without the dimensionless correction factor for thick bundles $\frac{\nu}{\mu_1^+ + \mu_1^-}$ the forces due to the interaction of anti-parallel actin filaments are proportional to the product $\mu_1^+\,\mu_1^-$. With the correction factor of course the dependence is again different and essentially linear.

The appearance of the third moment $\mu_3^{\pm}$ is the viscosity coefficient, however, is not intuitive. It is well know that the third moment of a distribution is related to the skewness of the distribution. However, in the present situation this fact does not help in the intuitive understanding of the role of $\mu_3^{\pm}$ in (18).

The third moment enters via the asymptotic results (14) and (15), where it appears due to the computation of the second moment in (32). That result refers to a situation with two filaments with given lengths and varying distance of their center points. It states, that if one integrates along the space of possible distances the square of these distances weighted by the length of the interaction region, then one obtains as a result products of first and third powers of these two lengths. As a consequence, after integrations with respect to these lengths against $\rho^{\pm}$, the respective moments appear in the limit equations (18). These observations, however, underline that the appearance of the third moments in the viscosity coefficient is a technical consequence when deriving the limit equation rather than something that one could also justify without going back to the microscopic model.

3.3. **Restriction to finite length.** In this section we will work with the system (10), (18) omitting the subscript $.0$ again. Note that it is still a model on the whole real line. In the following we restrict the actomyosin bundle to the time dependent interval

$$\Omega(t) := [x_0(t), x_1(t)]\,, \tag{19}$$

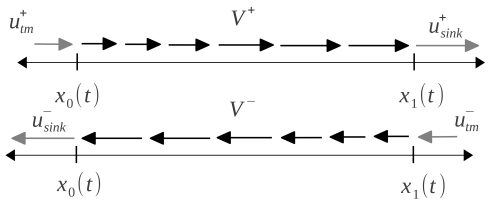

FIGURE 2. Velocity fields of right moving and left moving F-Actin respectively.

that is, from now on we consider the system (18)-(10) on the finite interval (19), the endpoints of which may vary with time. However, it now has to be complemented by boundary data.

To this end we assume that the exterior forces f^+ have negative sign for all $x \in (-\infty, x_0)$ and are zero otherwise, furthermore that f^- have positive sign for all $x \in (x_1, \infty)$ being zero otherwise. Additionally we assume that there is no myosin-II and no cross-linker proteins outside of $\Omega(t)$, where the corresponding coefficients η^{myo} and η^{cl} disappear.

The reasoning behind is that we describe external forces due to existing linkages with the cytoskeleton which tear those right moving filaments which are still not incorporated into the bundle to the left. Likewise the left moving filaments too are held back by external forces as long as they are not incorporated into the bundle at the right tip. On the other hand we do not want to describe forces which act on those actin filaments that already have passed the bundle and left it, neither external forces nor forces transmitted by cross-linkers or molecular motors. Observe that after these fibers were exposed to polymerization during their passage through the bundle only few such fibers will exists when they arrive at the opposed end point of the bundle.

The external forces are then aggregated according to

$$
\begin{aligned}
F^+_{\mathrm{left}}(t) &:= -\int_{-\infty}^{x_0(t)} \int_0^\infty f^+(t,x,l)\, \rho_1^+(t,x,l)\, dl\, dx \geq 0 \quad \text{and} \\
F^-_{\mathrm{right}}(t) &:= \int_{x_1(t)}^{\infty} \int_0^\infty f^-(t,x,l)\, \rho_1^-(t,x,l)\, dl\, dx \geq 0\,,
\end{aligned}
\tag{20}
$$

where F^+_{left} represents the total of forces which hold back the right moving actin filaments at the left tip of the bundle. In the same way F^-_{right} is the force which holds back the left moving filaments at the right tip of the bundle.

We integrate (18) on $(-\infty, x_0)$ and (x_1, ∞) respectively to obtain

$$
\begin{aligned}
F^+_{\mathrm{left}} &= \eta^{\mathrm{bdl}} \frac{1}{12}\, \frac{\nu \mu_3^+ \mu_1^+}{\mu_1^+ + \mu_1^-} \partial_x V^+\Big|_{x_0(t)} & 0 &= \partial_x V^+\Big|_{x_1(t)} \\
0 &= \partial_x V^-\Big|_{x_0(t)} & F^-_{\mathrm{right}} &= \eta^{\mathrm{bdl}} \frac{1}{12}\, \frac{\nu \mu_3^- \mu_1^-}{\mu_1^+ + \mu_1^-} \partial_x V^-\Big|_{x_1(t)}
\end{aligned}
\tag{21}
$$

Observe that by integration of (18) this implies

$$
F^+_{\mathrm{left}} = F^-_{\mathrm{right}} = \int_{x_0(t)}^{x_1(t)} \left(\eta^{\mathrm{myo}} - \eta^{\mathrm{cl}} \left(V^+ - V^-\right)\right) \frac{\nu \mu_1^+ \mu_1^-}{\mu_1^+ + \mu_1^-}\, dx\,. \tag{22}
$$

Additionally new F-Actin is delivered into the bundle by the rear flow in the cytosol. It is modeled as an inflow of right moving filaments at $x_0(t)$ with tread-milling speed $u_{\text{left}}^{\text{tm}+}(t)$ and length distribution $\rho_{\text{left}}^{+\text{tm}}(t,l)$. At the same time there is an inflow of left going filaments at the right boundary with speed $u_{\text{right}}^{\text{tm}-}$ and length distribution $\rho_{\text{right}}^{-\text{tm}}$. These statements lead to the boundary data for the continuum equations (10) and the free boundary conditions which define the dynamics of the boundaries of $\Omega(t)$,

$$\partial_t x_0(t) = V^+(x_0(t)) - u_{\text{left}}^{\text{tm}+}(t) \qquad \partial_t x_1(t) = V^-(x_1(t)) + u_{\text{right}}^{\text{tm}-}(t) \tag{23}$$

$$\rho^+(t, x_0(t), l) = \rho_{\text{left}}^{+\text{tm}}(t,l) \qquad \rho^-(t, x_1(t), l) = \rho_{\text{right}}^{-\text{tm}}(t,l) \tag{24}$$

for all $l \geq 0$. The situation is summarized in figure 2. In this figure

$$u_{\text{sink}}^+ := V^+(x_1(t)) + \partial_t x_1(t) \quad \text{and} \quad u_{\text{sink}}^- := V^-(x_0(t)) - \partial_t x_0(t) \tag{25}$$

represent the fluxes by which F-Actin, which was not depolymerized during its trajectory through the bundle, is transported out of the bundle.

We remark that a similar boundary condition was formulated in [2], yet in combination with other terms that couple the boundary value of the velocity field with dependent quantities. The present model is simpler in that the boundary value of the velocity field on one side is basically directly given by the tread-milling/retrograde-flow rates $u_{\text{left}}^{\text{tm}+}$ and $u_{\text{right}}^{\text{tm}-}$. The idea behind is that the bundle also exists outside of $[x_0, x_1]$, where it is closely linked to/part of the cytoskeleton. Through this close integration of bundle and cytoskeleton the retrograde flow rate is imposed as the boundary data of the velocity fields in the bundle.

4. Conceptions of model formulation, boundary data

The model consisting of equations (10) and (18) stated on $\Omega(t) = [x_0(t), x_1(t)]$ and the conditions (21), (23) and (24) is actually overdetermined. We identify primarily two approaches to formulate it as a well posed model.

(1) One is to assume that the positions of the boundaries are known parameter functions, in fact they might be given constants. The forces acting at the tips of the bundle according to (21) are then part of the solution of the model.
(2) The second approach is to fix the (time-dependent) forces at the tip of the bundle using (21) as boundary data. The dynamics of the tips is then part of the solution of the model and given by (23).

In the following we present both approaches to formulate the model in more detail.

4.1. **Fixed boundary model to compute contractile forces.**

We assume that the positions of the boundaries are known parameter functions, in fact they might be given constants. In this case one solves the following problem on $\Omega(t)$

$$\begin{cases} 0 = \partial_t \rho^\pm + \partial_x \left(V^\pm \rho^\pm \right) + \partial_{l^\pm} \left(G^\pm \rho^\pm \right) , \\ \rho^+(t, x_0(t), .) = \rho_{\text{left}}^{+\text{tm}}(t, .) , \\ \rho^-(t, x_1(t), .) = \rho_{\text{right}}^{-\text{tm}}(t, .) , \end{cases} \tag{26}$$

coupled to

$$
(27)\qquad \begin{cases} 0 = \dfrac{\eta^{\mathrm{bdl}}}{12}\,\partial_x\left(\dfrac{\nu\mu_1^{\pm}\mu_3^{\pm}}{\mu_1^{+}+\mu_1^{-}}\partial_x V^{\pm}\right) \pm \left(\eta^{\mathrm{myo}} - \eta^{\mathrm{cl}}\left(V^{+}-V^{-}\right)\right)\dfrac{\nu\mu_1^{+}\mu_1^{-}}{\mu_1^{+}+\mu_1^{-}}\ , \\ V^{+}(x_0(t)) = \partial_t x_0(t) + u_{\mathrm{left}}^{\mathrm{tm}+}(t)\ , \\ \partial_x V^{-}(x_0(t)) = 0\ , \\ V^{-}(x_1(t)) = \partial_t x_1(t) - u_{\mathrm{right}}^{\mathrm{tm}-}(t)\ , \\ \partial_x V^{+}(x_1(t)) = 0\ . \end{cases}
$$

Based on a solution of this model we may compute the forces at the ends of the bundle according to the formulas given in (21). As an additional output of the model we also obtain the speed and amount of F-Actin material being pushed out of the bundle at the other tip given by (25) and $\rho^{\pm}$ at $x_0(t)$ and $x_1(t)$ respectively.

4.2. **Free boundary model given contractile forces.** Alternatively we may also assume that we know the forces at the boundaries $F_{\mathrm{left}}^{+} = F_{\mathrm{right}}^{-} > 0$ and replace the boundary conditions in (27) by (21) obtaining the following problem on $\Omega(t)$,

$$
(28)\qquad \begin{cases} 0 = \partial_t \rho^{\pm} + \partial_x\left(V^{\pm}\rho^{\pm}\right) + \partial_{l^{\pm}}\left(G^{\pm}\rho^{\pm}\right)\ , \\ \rho^{+}(t, x_0(t), .) = \rho_{\mathrm{left}}^{+\mathrm{tm}}(t, .)\ , \\ \rho^{-}(t, x_1(t), .) = \rho_{\mathrm{right}}^{-\mathrm{tm}}(t, .)\ , \end{cases}
$$

coupled to

$$
(29)\qquad \begin{cases} \eta^{\mathrm{fr}}\mu_1^{\pm}V^{\pm} = \dfrac{\eta^{\mathrm{bdl}}}{12}\,\partial_x\left(\dfrac{\nu\mu_1^{\pm}\mu_3^{\pm}}{\mu_1^{+}+\mu_1^{-}}\partial_x V^{\pm}\right) \pm \left(\eta^{\mathrm{myo}} - \eta^{\mathrm{cl}}\left(V^{+}-V^{-}\right)\right)\dfrac{\nu\mu_1^{+}\mu_1^{-}}{\mu_1^{+}+\mu_1^{-}}\ , \\ F_{\mathrm{left}}^{+}(t) = \eta^{\mathrm{bdl}}\dfrac{1}{12}\,\dfrac{\nu\mu_3^{+}\mu_1^{+}}{\mu_1^{+}+\mu_1^{-}}\partial_x V^{+}\Big|_{x_0(t)}\ , \\ \partial_x V^{-}(x_0(t)) = 0\ , \\ F_{\mathrm{right}}^{-}(t) = \eta^{\mathrm{bdl}}\dfrac{1}{12}\,\dfrac{\nu\mu_3^{-}\mu_1^{-}}{\mu_1^{+}+\mu_1^{-}}\partial_x V^{-}\Big|_{x_1(t)}\ , \\ \partial_x V^{+}(x_1(t)) = 0\ , \end{cases}
$$

where we added an additional term modeling friction with the cytoplasm with friction coefficient $\eta^{\mathrm{fr}} > 0$ in order to ensure uniqueness of solutions to (29), as the equation otherwise would be invariant with respect to adding an arbitrary constant to the tuple (V^{+}, V^{-}). As an output of the model we obtain the dynamics of the free boundary according to the formulas (23) and also the sink velocities (25).

5. Steady state solutions

We concentrate on the model for a bundle of fixed length (26)-(27) and look at steady state solutions, hence we assume that the parameters of the model do not depend on time.

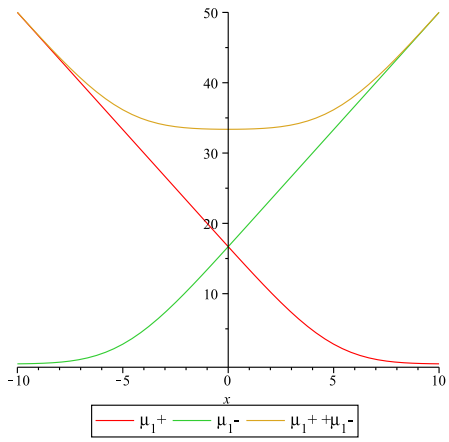

FIGURE 3. F-Actin distribution in the bundle according to the asymptotic solution when $\eta^{\rm bdl} \to \infty$.

There are two asymptotic regimes with respect to the activity of bundling proteins $\eta^{\rm bdl}$ in which the contractile force given by (22) can be computed explicitly.

The formal limit $\eta^{\rm bdl} \to 0$ in (27), i.e. the viscosity effect of bundling proteins becomes small, implies that $\eta^{\rm myo} - \eta^{\rm cl}\,(V^+ - V^-) = 0$. All the forces generated by myosin-II are hence immediately compensated by inter-filamentous drag forces and by (22) no contractile forces are acting at the tips of the bundle, $F^+_{\rm left} = F^-_{\rm right} = 0$.

The other asymptotic limit which allows to compute the contractile forces explicitly is attained when the effect of bundling proteins dominates, i.e. $\eta^{\rm bdl} \to \infty$. The system (27) then implies that the velocities $V^\pm$ are constant and are given by the tread-milling rates, i.e. $V^+ = u^{\rm tm+}_{\rm left}$ and $V^- = u^{\rm tm-}_{\rm right}$. In this case by evaluating (22) we obtain

$$F^+_{\rm left} = F^-_{\rm right} = \int_{x_0}^{x_1} \left(\eta^{\rm myo} - \eta^{\rm cl}\left(u^{\rm tm+}_{\rm left} - u^{\rm tm-}_{\rm right}\right)\right) \frac{\nu \mu_1^+ \mu_1^-}{\mu_1^+ + \mu_1^-}\, dx\,. \tag{30}$$

To compute $\mu_1^\pm$ we also assume that the depolymerization rates are homogeneous, i.e. $G^\pm(x,l) \equiv G^\pm$, which allows to write the steady state solution of the continuity equations (26) as

$$\begin{aligned} \rho^+(x,l) &= \rho^{+\rm tm}_{\rm left}(l + (x_0 - x)\, G^+/V^+)\,, \\ \rho^-(x,l) &= \rho^{-\rm tm}_{\rm right}(l + (x_1 - x)\, G^-/V^-)\,. \end{aligned}$$

We obtain

$$\begin{aligned} \mu_1^+(x) &= \int_0^\infty l\, \rho^{+\rm tm}_{\rm left}(l + (x_0 - x)\, G^+/V^+)\, dl\,, \\ \mu_1^-(x) &= \int_0^\infty l\, \rho^{-\rm tm}_{\rm right}(l + (x_1 - x)\, G^-/V^-)\, dl\,, \end{aligned} \tag{31}$$

which we visualize in figure 3 for the case of a bundle of length 20 μm with $x_0 = -10\ \mu m$ and $x_1 = 10\ \mu m$ and using the parameter values given in table 1.

Figure 3 also shows the sum of μ_1^+ and μ_1^- which represents the overall density of F-Actin per unit bundle length at a given position along the bundle. The observed

TABLE 1. List of parameters and literature sources.

Description	Symbol	Value	Reference
Depolymerization rate	$G^{\pm}$	$2\,\mu m\,\mathrm{min}^{-1}$	cf. [25]
Max. number of neighboring filaments	ν	6	cf. [35]
Tread-milling speed at the tips of the bundle	$u^{\mathrm{tm}+}_{\mathrm{left}}$, $u^{\mathrm{tm}-}_{\mathrm{right}}$	$6\,\mu m\,\mathrm{min}^{-1}$	estimate by the author
Effective force coefficient due to myosin-II heads	η^{myosin}	$24.5\,pN\,\mu m^{-1}$	see appendix B
Macrocopic drag friction due to cross-linkers	η^{cl}	$1.12\,pN\,\mathrm{min}\,\mu m^{-2}$	see appendix B
Length distribution of actin filaments flowing into the bundle	$\rho^{+\mathrm{tm}}_{\mathrm{left}} = \rho^{-\mathrm{tm}}_{\mathrm{right}}$	$\frac{10}{\sqrt{\pi}}\exp(-(l-5)^2)$	estimate: about 50 filaments with an average length of 5 μm

steady state is actually a dynamic equilibrium. The trajectory of a single right moving actin filament for example starts at x_0 where it enters the bundle. It is then transported to the right with velocity V^+ while depolymerizing with rate $G^{\pm} < 0$. The overall decay in concentration of right moving filaments from left the right and the decay in concentration of left moving filaments in the opposed direction is therefore a consequence of dominating depolymerization during the trajectory of every single actin filament (and potentially also of acceleration along their way through the bundle if η^{bdl} was finite).

Furthermore, again using the parameter values given in table 1, the contractile force according to (30) is given by $F^{+}_{\mathrm{left}} = F^{-}_{\mathrm{right}} = 4539.1\ pN$. This number is of course large given the facts that typical stall forces of lamellipodia are in the magnitude of $1000 - 1500\,pN$ ([29, 19]) and forces exerted by single barbed ends in the magnitude of $1 - 9\ pN$ ([14, 27]). In fact the above number should be seen as an upper limit to the actual contractile force of the bundle since we considered the limit of zero viscosity. We remark that without drag friction the contractile force would be about twice as large hence about half of the force generated by myosin-II filaments is compensated by drag friction caused by cross-linker proteins.

5.2. **Numerical computations.** Numerical computations for the case when η^{bdl} takes a finite value allow to obtain more realistic values. We expect that part of the total force computed above would be consumed by the viscosity caused by bundling proteins. In Figure 4 we use a numerical scheme to compute the contractile forces for different choices of the drag friction caused by bundling proteins.

We use a standard mass preserving upwind scheme for the time dependent continuity equations (26), while the elliptic equations (27) are discretized using a finite

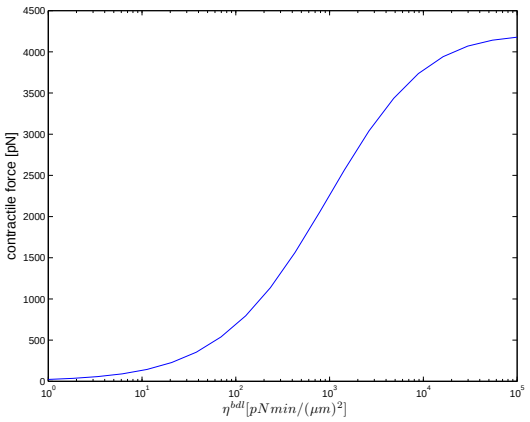

FIGURE 4. Numerical values of the contractile force $F^+_{\text{links}} = F^-_{\text{rechts}}$ of a stationary bundle as a function of the drag friction caused by bundling proteins η^{bdl}.

difference scheme, bot on regular grids. We then compute long time solutions with this time-dependent scheme in order to obtain numerical steady state solutions.

It turns out that when η^{bdl} is of the magnitude of about $120\,pN\,\text{min}\,\mu m^{-2}$ we obtain values of the contractile force in the realistic range of $1000 - 1500\,pN$. Otherwise, if η^{bdl} becomes very small or very large, the contractile force will approach the asymptotic values $F^+_{\text{left}} = F^-_{\text{right}} = 0\,pN$ and $F^+_{\text{left}} = F^-_{\text{right}} = 4539.1\,pN$ (numerical errors prevent the numerical value to fully approach that value), respectively, which we have obtained by explicit computations in the preceding subsection.

6. Discussion

In this paper we investigate non-sarcomeric actomyosin bundles which are composed of polar actin filaments interspersed with bipolar myosin-II filaments. We formulate a mathematical model for a two-phase viscous fluid in one dimension. The two phases are composed of directed actin filaments with their barbed ends in either one of the two directions. We use a coarse-graining approach by which we consider the asymptotic limit of small actin filaments lengths. The model assumes that the bundle is in an over-damped state and combines force generation by myosin-II filaments, intrinsic friction as the macroscopic effect of cross-linking proteins and viscosity caused by bundling proteins. Finally external forces attach to the two tips of the bundle the positions of which may vary with time.

The model is formulated as a system of two continuum equations for the two phases of actin filaments coupled to two elliptic equations for the fluxes and boundary conditions to take into account the forces at the tips. Its solutions typically feature an anti-parallel F-Actin flow in the sense that the two phases of actin filaments move in opposite directions, namely in the direction of their pointed ends.

The model is very versatile and can be used in two ways. Either the size of the bundle is known, possibly varying over time, then the contractile forces can be computed given a solution to the model. Or, the forces at the tips are known, then

the model is treated as a free boundary problem such that the change in length is an outcome of evaluating the model.

In general, solutions to this PDE (partial differential equation)-model will be computed numerically which is not the scope of this study. Yet, in the case of fixed bundle length, the steady state solutions to two asymptotic limits of the model can be computed explicitly. The asymptotic regimes are the one of zero viscosity where no bundling proteins are present and the one where bundling proteins are abundant and viscosity grows very (infinitely) large.

In the first case the contractile force becomes zero showing that the effect of bundling proteins is crucial for the propagation of contractile forces to the tips. In the second case the contractile force converges to a finite value given by the total of the forces exerted by myosin-II filaments reduced by drag forces due to cross-linking proteins.

In this case we can compute the solution of the model explicitly obtaining $F = 4539.1\,pN$ as the contractile force generated by the bundle. This value should be seen as an upper limit to the actual contractile force exerted by the bundle when the effect of bundling proteins is limited and hence viscosity is present. Numerical fitting of a suitable value for η^{bdl} allows to obtain a more realistic value for the contractile force in the range of $1000 - 1500\ pN$. In a future study, numerical methods will be used to assess the behavior of the bundle under tension, where we expect contractile behavior ([28]). The formula (22) allows a straightforward analysis of the situation. It states that the total amount of forces generated by myosin are partly compensated by drag forces due to cross-linker proteins. The rest is then partially propagated to the tips of the bundle due to the viscosity in the model effected by bundling proteins.

Hence the model allows us to conclude that the presence of bundling proteins connecting parallel actin filaments is necessary for contractility because they transmit the locally generated forces to the tips.

Appendix A. Technical results used to derive the asymptotic limit

First we present a list of explicit expressions for the following moments of the length of the interacting region using the abbreviated notation $\bar{L}^{(x,\varepsilon l)}_{(\bar{x},\varepsilon\bar{l})} := L^{(x-\varepsilon l/2,x+\varepsilon l/2)}_{(\bar{x}-\varepsilon\bar{l}/2,\bar{x}+\varepsilon\bar{l}/2)}$.

$$
\begin{aligned}
\int_{\mathbb{R}} \bar{L}^{(0,\varepsilon l)}_{(\Delta\bar{x},\varepsilon\bar{l})}\, d\Delta\bar{x} &= \varepsilon^2\, \bar{l}\, l\ , \\
\int_{\mathbb{R}} \Delta\bar{x}\, \bar{L}^{(0,\varepsilon l)}_{(\Delta\bar{x},\varepsilon\bar{l})}\, d\Delta\bar{x} &= 0\ , \\
\int_{\mathbb{R}} (\Delta\bar{x})^2 \bar{L}^{(0,\varepsilon l)}_{(\Delta\bar{x},\varepsilon\bar{l})}\, d\Delta\bar{x} &= \frac{\varepsilon^4}{12}\, \bar{l}\, l\, (l^2+\bar{l}^2)\ .
\end{aligned}
\tag{32}
$$

Next, we compute the first order expansion of the effective interaction length. We consider (2) formulated in terms of density functions after scaling,

$$
N^{(\alpha,\beta)} = \frac{1}{\beta-\alpha}\frac{1}{\varepsilon}\int_{\mathbb{R}}\int_0^\infty \bar{L}^{((\alpha+\beta)/2,\beta-\alpha)}_{(x+\Delta\tilde{x},\tilde{l})}(\rho^+(t,x+\Delta\tilde{x},\tilde{l})+\rho^-(t,x+\Delta\tilde{x},\tilde{l}))\, d\tilde{l}\, d\Delta\tilde{x}\ .
$$

We use the short notation $\bar\rho(t,x,l) := \rho^+(t,x,l) + \rho^-(t,x,l)$ and apply a Taylor expansion up to first order to obtain

$$\begin{aligned}
N^{(\alpha,\beta)} &\approx \frac{1}{\beta-\alpha}\frac{1}{\varepsilon}\int_{\mathbb{R}}\int_0^\infty \bar L^{((\alpha+\beta)/2,\beta-\alpha)}_{(x+\Delta\tilde x,\varepsilon\tilde l)}\left(\bar\rho(t,x,\tilde l)+\Delta\tilde x\,\partial_x\bar\rho(t,x,\tilde l)\right)\,d\tilde l\,d\Delta\tilde x = \\
&= \frac{1}{\beta-\alpha}\frac{1}{\varepsilon}\int_{\mathbb{R}}\int_0^\infty \bar L^{(0,\beta-\alpha)}_{(x-(\alpha+\beta)/2+\Delta\tilde x,\varepsilon\tilde l)}\left(\bar\rho(t,x,\tilde l)+\Delta\tilde x\,\partial_x\bar\rho(t,x,\tilde l)\right)\,d\tilde l\,d\Delta\tilde x = \\
&= \frac{1}{\beta-\alpha}\frac{1}{\varepsilon}\int_{\mathbb{R}}\int_0^\infty \bar L^{(0,\beta-\alpha)}_{(\Delta\tilde y,\varepsilon\tilde l)}\left(\bar\rho(t,x,\tilde l)+\left(\frac{\alpha+\beta}{2}-x+\Delta\tilde y\right)\partial_x\bar\rho(t,x,\tilde l)\right)\,d\tilde l\,d\Delta\tilde y = \\
&= \frac{1}{\beta-\alpha}\frac{1}{\varepsilon}\int_0^\infty (\beta-\alpha)\,\varepsilon\,\tilde l\,\left(\bar\rho(t,x,\tilde l)+\left(\frac{\alpha+\beta}{2}-x\right)\partial_x\bar\rho(t,x,\tilde l)\right)\,d\tilde l = \\
&= \left(\mu_1^+(t,x)+\mu_1^-(t,x)+\left(\frac{\alpha+\beta}{2}-x\right)\left(\partial_x\mu_1^+(t,x)+\partial_x\mu_1^-(t,x)\right)\right)\,,
\end{aligned}$$

where we used the results for the zeroth and the first moments in (32). This implies that the approximation of the effective interaction length up to first order terms is given by

$$\begin{aligned}
(33)\quad \bar A^{(x,\varepsilon l)}_{(x+\Delta\bar x,\varepsilon\bar l)} = \bar L^{(x,\varepsilon l)}_{(x+\Delta\bar x,\varepsilon\bar l)}\frac{\nu}{N^{(\alpha,\beta)}} \approx \bar L^{(0,\varepsilon l)}_{(\Delta\bar x,\varepsilon\bar l)}\Bigg(&\frac{\nu}{\mu_1^+(t,x)+\mu_1^-(t,x)} - \\
&-\frac{\nu}{(\mu_1^+(t,x)+\mu_1^-(t,x))^2}\left(\frac{\alpha+\beta}{2}-x\right)\left(\partial_x\mu_1^+(t,x)+\partial_x\mu_1^-(t,x)\right)\Bigg)\,,
\end{aligned}$$

where $\alpha := \max(x-\epsilon l/2, x+\Delta\bar x-\epsilon\bar l/2)$, $\beta := \min(x+\epsilon l/2, x+\Delta\bar x+\epsilon\bar l/2)$. This result is complemented by the fact that

$$\int_{\mathbb{R}}\Delta\bar x\left(\frac{\alpha+\beta}{2}-x\right)\bar L^{(0,\varepsilon l)}_{(\Delta\bar x,\varepsilon\bar l)}\,d\Delta\bar x = \frac{\varepsilon^4}{12}\,\bar l\,l^3\,.$$

Appendix B. Derivation of effective parameters

The computation of the effective contractile force due to myosin-II filaments η^{myosin} interspersed between actin filaments relates to known data for the force exerted by single myosin-II heads $\kappa^{\text{myosin}} = 3.5\,pN$ ([13]) and the space between myosin-II heads (cf. [40]) which allows to estimate the maximal number of myosin heads interacting with F-Actin by $\rho^{\text{myosin}}_{\max} = 1/(0.0145\,\mu m) \approx 70\,\mu m^{-1}$. We additionally take into account a fixed saturation factor which we estimate as $s^{\text{myosin}} = 10\%$ and compute the macroscopic parameter according to

$$\eta^{\text{myosin}} = \kappa^{\text{myosin}}\rho^{\text{myosin}}_{\max}s^{\text{myosin}}\,.$$

The derivation of the other macroscopic parameter η^{cl} which we use in the evaluation of (30) is motivated by a microscopic model ling approach which was first introduced in [26]. We assume that only α-actinin acts as a cross-linker. It is a homo-dimer of about $35\,nm$ length ([32]) and able to cross-link all orientations of actin filaments ([9]). From a linear fit of data in [12] we obtain the stretching elasticity of α-actinin modeled as an elastic spring $\kappa^{\alpha\text{-actinin}} = 100\,pN\,\mu m^{-1}$. From [38] we take the off-rate of F-Actin bound α-actinin $\zeta^{\alpha\text{-actinin}} = 5.2\,\text{sec}^{-1}$ the reciprocal of which is the typical duration of a linkage. As an estimate we use the same value as for myosin-II for the maximal density of α-actinin linkages on F-Actin $\rho^{\alpha\text{-actinin}}_{\max} = 70\,\mu m^{-1}$. We estimate the saturation factor as half the value

of myosin, $s^{\alpha\text{-actinin}} = 5\%$, taking into account the large off-rate of α-actinin and the fact that myosin forms bipolar filaments. Finally the macroscopic drag friction coefficient due to cross-linker proteins is computed by

$$\eta^{\mathrm{cl}} = \kappa^{\alpha\text{-actinin}} \frac{1}{\zeta^{\alpha\text{-actinin}}} \, \rho_{\max}^{\alpha\text{-actinin}} \, s^{\alpha\text{-actinin}} \, .$$

Although we do not use a physical value of η^{bdl} in the computations in Section 5, we state for completeness the analogous formula that would allow to derive this coefficient from microscopic data on fascin,

$$\eta^{\mathrm{bdl}} := \kappa^{\mathrm{fascin}} \frac{1}{\zeta^{\mathrm{fascin}}} \rho_{\max}^{fascin} s^{\mathrm{fascin}} \, .$$

Acknowledgement

This work has been supported by the Vienna Science and Technology Fund (WWTF) through the project "Mathematical modeling of actin driven cell migration" of C. Schmeiser.

References

1. B. Alberts, A. Johnson, J. Lewis, M. Raff, K. Roberts, and P. Walter, *Molecular biology of the cell*, Garland Science, New York, 2002.
2. Wolfgang Alt, Martin Bock, and Christoph Möhl, *Coupling of cytoplasm and adhesion dynamics determines cell polarization and locomotion.*, Cell mechanics: from single scale-based models to multiscale modelling (A. Chauviere, L. Preziosi, and C. Verdier, eds.), Chapman & Hall/CRC Mathematical & Computational Biology, Chapman and Hall / CRC Press, 2010.
3. Wolfgang Alt and Micah Dembo, *Cytoplasm dynamics and cell motion: Two-phase flow models.*, Math. Biosci. **156** (1999), no. 1-2, 207–228.
4. D.E. Bentil, *Modelling and simulation of motility in actomyosin systems*, Journal of Computational Biology **5** (1998), no. 1, 73–86.
5. A Besser and U S Schwarz, *Coupling biochemistry and mechanics in cell adhesion: a model for inhomogeneous stress fiber contraction*, New Journal of Physics **9** (2007), no. 11, 35.
6. Achim Besser, Julien Colombelli, Ernst H. K. Stelzer, and Ulrich S. Schwarz, *Viscoelastic response of contractile filament bundles*, Phys. Rev. E **83** (2011), 051902.
7. Ana Carvalho, Arshad Desai, and Karen Oegema, *Structural memory in the contractile ring makes the duration of cytokinesis independent of cell size*, Cell **137** (2009), no. 5, 926 – 937.
8. Julien Colombelli, Achim Besser, Holger Kress, Emmanuel G Reynaud, Philippe Girard, Emmanuel Caussinus, Uta Haselmann, John V Small, Ulrich S Schwarz, and Ernst H K Stelzer, *Mechanosensing in actin stress fibers revealed by a close correlation between force and protein localization.*, Journal of Cell Science **122** (2009), no. Pt 10, 1665–1679.
9. D.S. Courson and R.S. Rock, *Actin cross-link assembly and disassembly mechanics for α-actinin and fascin*, Journal of Biological Chemistry **285** (2010), no. 34, 26350–26357.
10. Louise P. Cramer, Margaret Siebert, and Timothy J. Mitchison, *Identification of novel graded polarity actin filament bundles in locomoting heart fibroblasts: Implications for the generation of motile force*, The Journal of Cell Biology **136** (1997), no. 6, 1287–1305.
11. F S Fay, K Fujiwara, D D Rees, and K E Fogarty, *Distribution of alpha-actinin in single isolated smooth muscle cells.*, The Journal of Cell Biology **96** (1983), no. 3, 783–795.
12. Jorge M. Ferrer, Hyungsuk Lee, Jiong Chen, Benjamin Pelz, Fumihiko Nakamura, Roger D. Kamm, and Matthew J. Lang, *Measuring molecular rupture forces between single actin filaments and actin-binding proteins*, Proceedings of the National Academy of Sciences (2008).
13. J.T. Finer, R.M. Simmons, and J.A. Spudich, *Single myosin molecule mechanics: Piconewton forces and nanometre steps*, Nature **368** (1994), no. 6467, 113–119.
14. Matthew J. Footer, Jacob W. J. Kerssemakers, Julie A. Theriot, and Marileen Dogterom, *Direct measurement of force generation by actin filament polymerization using an optical trap*, Proceedings of the National Academy of Sciences **104** (2007), no. 7, 2181–2186.

15. Gregory M. Grason and Homin Shin, *Structural reorganization of parallel actin bundles by crosslinking proteins: Incommensurate states of twist*, Biophysical Journal **100** (2011), no. 3, Supplement 1, 34a – 34a.
16. A. Huxley, *Muscle structure and theories of contraction.*, Prog Biophys Biophys Chem **7** (1957), 255–318.
17. Asier Jayo and Maddy Parsons, *Fascin: A key regulator of cytoskeletal dynamics*, The International Journal of Biochemistry & Cell Biology **42** (2010), no. 10, 1614 – 1617.
18. K. Katoh, Y. Kano, M. Masuda, H. Onishi, and K. Fujiwara, *Isolation and contraction of the stress fiber*, Molecular Biology of the Cell **9** (1998), no. 7, 1919–1938.
19. Michael M. Kozlov and Alex Mogilner, *Model of polarization and bistability of cell fragments*, Biophysical Journal **93** (2007), no. 11, 3811 – 3819.
20. K. Kruse and F. Jülicher, *Actively contracting bundles of polar filaments*, Phys. Rev. Lett. **85** (2000), 1778–1781.
21. Karsten Kruse and Frank Jülicher, *Self-organization and mechanical properties of active filament bundles*, Phys. Rev. E **67** (2003), 051913.
22. G. Langanger, M. Moeremans, and G. Daneels, *The molecular organization of myosin in stress fibers of cultured cells*, Journal of Cell Biology **102** (1986), no. 1, 200–209.
23. Martin Lenz, Margaret L. Gardel, and Aaron R. Dinner, *Requirements for contractility in disordered cytoskeletal bundles*, New Journal of Physics **14** (2012), no. 3, 033037.
24. F.C. Mackintosh and A.J. Levine, *Nonequilibrium mechanics and dynamics of motor-activated gels*, Physical Review Letters **100** (2008), no. 1.
25. A. Mogilner and L. Edelstein-Keshet, *Regulation of actin dynamics in rapidly moving cells: A quantitative analysis*, Biophysical Journal **83** (2002), no. 3, 1237–1258.
26. Dietmar Oelz and Christian Schmeiser, *Derivation of a model for symmetric lamellipodia with instantaneous cross-link turnover*, Arch. Ration. Mech. Anal. **198** (2010), no. 3, 963–980.
27. C.S. Peskin, G.M. Odell, and G.F. Oster, *Cellular motions and thermal fluctuations: the brownian ratchet*, Biophysical Journal **65** (1993), no. 1, 316 – 324.
28. Lynda J. Peterson, Zenon Rajfur, Amy S. Maddox, Christopher D. Freel, Yun Chen, Magnus Edlund, Carol Otey, and Keith Burridge, *Simultaneous stretching and contraction of stress fibers in vivo*, Molecular Biology of the Cell **15** (2004), no. 7, 3497–3508.
29. Marcus Prass, Ken Jacobson, Alex Mogilner, and Manfred Radmacher, *Direct measurement of the lamellipodial protrusive force in a migrating cell*, The Journal of Cell Biology **174** (2006), no. 6, 767–772.
30. O.M. Rossier, N. Gauthier, N. Biais, W. Vonnegut, M.-A. Fardin, P. Avigan, E.R. Heller, A. Mathur, S. Ghassemi, M.S. Koeckert, J.C. Hone, and M.P. Sheetz, *Force generated by actomyosin contraction builds bridges between adhesive contacts*, EMBO Journal **29** (2010), no. 6, 1055–1068.
31. B. Rubinstein, K. Fournier, M.F.and Jacobson, A.B. Verkhovsky, and A. Mogilner, *Actin-myosin viscoelastic flow in the keratocyte lamellipod*, Biophysical Journal **97** (2009), no. 7, 1853–1863.
32. Reza Sharifi Sedeh, Alexander A. Fedorov, Elena V. Fedorov, Shoichiro Ono, Fumio Matsumura, Steven C. Almo, and Mark Bathe, *Structure, evolutionary conservation, and conformational dynamics of homo sapiens fascin-1, an f-actin crosslinking protein*, Journal of Molecular Biology **400** (2010), no. 3, 589 – 604.
33. Tatyana M. Svitkina, Alexander B. Verkhovsky, Kyle M. McQuade, and Gary G. Borisy, *Analysis of the actin-myosin ii system in fish epidermal keratocytes: Mechanism of cell body translocation*, The Journal of Cell Biology **139** (1997), no. 2, 397–415.
34. T. Thoresen, M. Lenz, and M.L. Gardel, *Reconstitution of contractile actomyosin bundles*, Biophysical Journal **100** (2011), no. 11, 2698–2705.
35. Y. Tseng, B.W. Schafer, S.C. Almo, and D. Wirtz, *Functional synergy of actin filament cross-linking proteins*, Journal of Biological Chemistry **277** (2002), no. 28, 25609–25616.
36. Yiider Tseng, Elena Fedorov, J.Michael McCaffery, Steven C Almo, and Denis Wirtz, *Micromechanics and ultrastructure of actin filament networks crosslinked by human fascin: A comparison with α-actinin*, Journal of Molecular Biology **310** (2001), no. 2, 351 – 366.
37. AB Verkhovsky, TM Svitkina, and GG Borisy, *Polarity sorting of actin filaments in cytochalasin-treated fibroblasts*, J Cell Sci **110** (1997), no. 15, 1693–1704.
38. D.H. Wachsstock, W.H. Schwarz, and T.D. Pollard, *Cross-linker dynamics determine the mechanical properties of actin gels*, Biophysical Journal **66** (1994), no. 3, Part 1, 801 – 809.

39. Robert R. Weihing, *The filamins: properties and functions*, Canadian Journal of Biochemistry and Cell Biology **63** (1985), no. 6, 397–413.
40. J.-Q. Xu, B.A. Harder, P. Uman, and R. Craig, *Myosin filament structure in vertebrate smooth muscle*, Journal of Cell Biology **134** (1996), no. 1, 53–66.

Dietmar Oelz, Johann Radon Institute for Computational and Applied Mathematics (RICAM),, "Mathematical Methods in Molecular and Systems Biology"-Group,, Apostelgasse 23, 1030 Vienna, Austria

E-mail address: dietmar.oelz@oeaw.ac.at